Magnetic susceptibility of disordered nondiffusive mesoscopic systems

Edward McCann* and Klaus Richter
Max-Planck-Institut für Physik komplexer Systeme, Nöthnitzer Strasse 38, 01187 Dresden, Germany
(Received 12 October 1998; revised manuscript received 8 January 1999)

Disorder-induced spectral correlations of mesoscopic quantum systems in the nondiffusive regime, and their effect on the magnetic susceptibility, are studied. We perform impurity averaging for nontranslational invariant systems by combining a diagrammatic perturbative approach with semiclassical techniques. This allows us to study the entire range from clean to diffusive systems. As an application we consider the magnetic response of noninteracting electrons in microstructures in the presence of weak disorder. We show that in the ballistic case (an elastic mean free path l larger than the system size) there exist two distinct regimes of behavior depending on the relative magnitudes of l and an inelastic scattering length L_ϕ. We present numerical results for square billiards, and derive approximate analytical results for generic chaotic geometries. The magnetic-field dependence and the L_ϕ dependence of the disorder-induced susceptibility are qualitatively similar in both types of geometry. [S0163-1829(99)02020-2]

I. INTRODUCTION

Mesoscopic physics has traditionally involved the study of phenomena in phase-coherent, disordered conductors.[1] In the diffusive regime, where the elastic mean free path l is much smaller than the system size L, the electron motion resembles that of a random walk between impurities.

The more recent development of high-mobility semiconductor heterostructures together with advanced lithographic techniques has led to the confinement of electrons in two-dimensional microstructures of controllable, nonrandom geometry. Thereby, a further regime, coined ''ballistic'' since $l>L$ has been realized. Such technological achievements have motivated theoretical approaches where the actual microcavities are approximated by ''clean'' quantum billiards, ignoring impurity scattering completely. In these models the electron motion is only affected by bounces at the confinement potential, which is the opposite case to the diffusive regime where confinement effects are not important on time scales shorter than the Thouless time.

However, residual impurity scattering is nearly unavoidable even in high-mobility microstructures. It has been shown that weak disorder can be strong enough to mix energy levels, influence spectral statistics,[2,3] and affect related thermodynamic quantities[4] in the ''ballistic'' regime.

In defining spectral correlation functions in the ''ballistic'' regime, one has to distinguish between disorder averaging, which we denote by $\langle\cdots\rangle_d$, and size averaging, $\langle\cdots\rangle_L$, which we assume to be equivalent to energy averaging. Pure disorder averaging corresponds to the experimental situation of an ensemble of weakly disordered microstructures of the same size. Recent work has shown that for this case spectral correlation functions contain, and are often dominated by, strong oscillatory structures in energy (on scales $k_F L$, k_F being the Fermi wave number) reflecting the presence of the confinement.[3,4] They can be semiclassically interpreted as density-of-states oscillations related to classical periodic orbits of the corresponding clean system.

In the present work we consider spectral correlations after both energy and (independent) disorder averaging corresponding to the experimental situation of an ensemble of disordered systems with variation in their sizes. Then one is able to divide the two-level correlation function $K(\varepsilon_1,\varepsilon_2)$, into two separate terms,[3,5]

$$K(\varepsilon_1,\varepsilon_2;H)\equiv\langle K^d(\varepsilon_1,\varepsilon_2;H)\rangle_L+K^L(\varepsilon_1,\varepsilon_2;H). \quad (1)$$

Here

$$K^d(\varepsilon_1,\varepsilon_2)=[\langle\nu(\varepsilon_1)\nu(\varepsilon_2)\rangle_d-\langle\nu(\varepsilon_1)\rangle_d\langle\nu(\varepsilon_2)\rangle_d]/\overline{\nu^2}, \quad (2a)$$

$$K^L(\varepsilon_1,\varepsilon_2)=\langle\langle\nu(\varepsilon_1)\rangle_d\langle\nu(\varepsilon_2)\rangle_d\rangle_L/\overline{\nu^2}-1, \quad (2b)$$

where ν denotes the single-particle density of states and $\overline{\nu}=\langle\langle\nu(\varepsilon)\rangle_d\rangle_L$ its mean part. K^d is a measure of *disorder-induced* correlations of the density of states, while K^L is given by *size-induced* correlations. In a diffusive system, $l<L$, the disorder-averaged density of states $\langle\nu(\varepsilon)\rangle_d$ is a constant, so that K^L is vanishingly small and K^d dominates. However, for $l>L$ the density of states contains terms which oscillate like $\cos(k_F L)$, and both correlation functions may be relevant. In contrast, once $l>L(k_F L)^{d-1}$, disorder-induced mixing of levels is negligible and K^L prevails.

The orbital magnetism of mesoscopic quantum systems is sensitive to spectral correlations as, e.g., measured by $K(\varepsilon_1,\varepsilon_2)$, and therefore has been the subject of much theoretical interest[6] as well as experimental investigations.[7–9] For isolated systems with a fixed number of particles it is necessary to consider averaging under canonical conditions,[10–12] resulting in a large contribution to the average magnetic response which can be by orders of magnitude larger than the (bulk) Landau diamagnetism. The corresponding susceptibility is given by[12]

$$\langle\chi(H)\rangle=-\left(\frac{\Delta}{2}\right)\frac{\partial^2}{\partial H^2}\langle\delta N^2(\mu;H)\rangle \quad (3)$$

for temperatures $k_B T$ larger than the mean level spacing Δ. In Eq. (3), H is the magnetic field and $\langle\delta N^2(\mu;H)\rangle$ is the variance in the number of energy levels within an energy

interval of width equal to the chemical potential, μ. This variance is related to $K(\varepsilon_1,\varepsilon_2;H)$ [Eq. (1)], by integration of the level energies ε_1 and ε_2 over the energy interval. Throughout this work we will label the contributions to the susceptibility, corresponding to $\langle K^d\rangle_L$ and K^L, as $\langle\chi^d(H)\rangle$ and $\langle\chi^L(H)\rangle$, respectively. Hence the total orbital magnetic susceptibility is composed of

$$\langle\chi(H)\rangle=\langle\chi^d(H)\rangle+\langle\chi^L(H)\rangle. \tag{4}$$

Diagrammatic techniques to treat impurity scattering are usually designed for diffusive systems, $l<L$, and therefore rely on the assumption of translational invariance. In this paper we combine a diagrammatic perturbation approach with semiclassical techniques to perform energy and impurity averaging and to calculate the disorder-induced part of the energy correlation function and the related susceptibility $\langle\chi^d(H)\rangle$ for disordered microstructures in the nondiffusive regime. In this quantum-semiclassical hybrid approach, scattering at the impurity potentials, which are assumed to be δ-like, is treated quantum mechanically in a perturbation series with respect to the disorder. Boundary effects are incorporated into a semiclassical representation of the Green functions, which enter into the impurity diagrams, in terms of classical paths. This method, therefore, takes into account, in a systematic way, contributions from (closed) trajectories which involve both scattering at impurities and specular reflection at the confinement potential. The procedure allows us to study the complete crossover from diffusive to clean systems. A preliminary brief account of this work has been presented in Ref. 5.

Our approach carries features of the ''method of trajectories'' originally devised for thin superconducting films.[13] Note that similar,[14] and alternative,[15] methods have been also employed to consider weak localization in thin films in a parallel magnetic field. Related semiclassical approaches for diffusive systems were proposed by Chakravarty and Schmid[16] and Argaman, Imry, and Smilansky.[17] More recently, Agam and Fishman[18] studied the spectral form factor for ballistic systems with rigid disks (spheres) as impurities from a quantum chaos point of view. We further note that a nonperturbative approach for ballistic systems has been developed by Muzykantskii and Khmelnitskii: the ballistic σ model.[19]

For real systems, besides l, there are additional relevant length scales at which inelastic scattering (L_ϕ) or temperature smearing (L_T) produce a damping of propagation. For clarity, in the following we refer to such a length scale as L_ϕ, although we assume that similar general arguments will hold for finite L_T. For ballistic motion at the Fermi energy E_F, we can relate L_ϕ to the level broadening γ by

$$\frac{L_\phi}{L}=\frac{k_FL}{2\pi}\frac{\Delta}{\gamma}. \tag{5}$$

This divides the ''ballistic'' regime into two subregimes. In the first, $L,L_\phi<l$, the particle motion is nearly ballistic: the damping (of the Green function) due to inelastic scattering typically occurs before elastic impurity scattering; for the remainder of this paper we refer to this regime as *inelastic*. In the second regime, $L<l<L_\phi$, a particle may scatter many times off impurities before scattering inelastically. We call this regime *elastic*. In our semiclassical treatment we consider the contribution of orbits *of all lengths* (smaller than v_Ft_H, where $t_H\approx\hbar/\Delta$ is the Heisenberg time) in both the elastic and inelastic regimes.

We present and compare results for noninteracting ballistic quantum systems with integrable and chaotic classical dynamics in the clean limit. We derive analytical estimates for the average susceptibility $\langle\chi^d(H)\rangle$ of generic chaotic microstructures, assuming ergodicity for the classical paths involved. As an example of an integrable geometry, we treat in detail the representative case of the square billiard. Experiments[9] on the magnetic susceptibility of ensembles of squares were performed in the ''ballistic'' inelastic regime, motivating theoretical studies of the susceptibility for $L<l$.[4,20] Gefen, Braun, and Montambaux[20] (GBM) considered the contribution of trajectories longer than l to $\langle\chi^d(H)\rangle$ in an approximate way, finding a paramagnetic l-independent contribution at zero field, whereas Richter, Ullmo, and Jalabert[4] (RUJ) calculated $\langle\chi^L(H)\rangle$ for a square by assuming that the disorder perturbs the phase, but not the trajectory, of semiclassical paths of the corresponding clean geometry. In the elastic regime we find agreement with the results of GBM with regard to the k_FL behavior, while the zero-field susceptibility is weakly dependent on l. In the inelastic regime, for larger level broadening, we find entirely different results, namely, an exponential dependence on L/L_ϕ and on L/l.

The present paper is organized as follows: In Sec. II we outline our combined semiclassical diagrammatic technique. In Sec. III we illustrate our approach by applying it to the case of integrable (square) billiards. We give analytical results for spectral correlation functions (at zero magnetic field) and numerical results for the magnetic susceptibility. In Sec. IV we present the derivation of the corresponding disorder-induced spectral correlations and susceptibility for chaotic ballistic geometries.

II. SEMICLASSICAL DIAGRAMMATIC APPROACH

In this section we summarize our semiclassical evaluation of the disorder correlation function K^d [Eq. (2a)], and the corresponding susceptibility $\langle\chi^d(H)\rangle$. To this end we begin with the diagrammatic formulation of the problem, and then perform the semiclassical approximations.

A. Diagrammatic framework

We consider noninteracting electrons in a weak, perpendicular magnetic field and a random Gaussian potential V, with $\langle V(\mathbf{r})\rangle=0$ and correlator

$$\langle V(\mathbf{r})V(\mathbf{r}')\rangle=\frac{\hbar}{2\pi\bar{\nu}\tau}\delta(\mathbf{r}-\mathbf{r}'), \tag{6}$$

describing white noise disorder. In Eq. (6), τ is the mean elastic scattering time, $l=v_F\tau$, and $\bar{\nu}=m/2\pi\hbar^2$ in two dimensions. In terms of the retarded and advanced single-

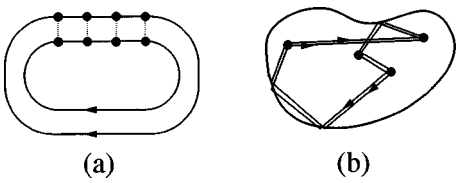

FIG. 1. The diagrams $\mathcal{S}_n^{(C)}$. (a) shows a schematic form of the diagram $\mathcal{S}_4^{(C)}$. (b) shows a pair of typical real space semiclassical trajectories which contribute to $\mathcal{S}_4^{(C)}$.

particle Green functions obeying the boundary conditions of the corresponding clean system, $\mathcal{G}^{+(-)}(\mathbf{r}_1,\mathbf{r}_2;\varepsilon;H)$, the correlator K^d may be written as

$$K^d(\varepsilon_1,\varepsilon_2;H)\approx\left(\frac{\Delta^2}{2\pi^2}\right)\mathcal{R}\langle\langle \mathrm{tr}\,\mathcal{G}^+(\varepsilon_1;H)\mathrm{tr}\,\mathcal{G}^-(\varepsilon_2;H)\rangle\rangle_d. \tag{7}$$

Here the average is taken over impurities only (for a given system size) and the symbol $\langle\langle\ldots\rangle\rangle_d$ implies the inclusion of connected diagrams only.

We are particularly interested in the field sensitive part, $\tilde{K}^d$, of K^d. Following a diagrammatic approach introduced in Ref. 3, this can be expressed as

$$\tilde{K}^d(\epsilon_1,\epsilon_2;H)=\frac{\Delta^2}{2\pi^2}\frac{\partial}{\partial\epsilon_1}\frac{\partial}{\partial\epsilon_2}\mathcal{R}\sum_{n=1}^{\infty}\frac{1}{n}\mathcal{S}_n^{(C)}(\omega;H), \tag{8}$$

with $\omega=\varepsilon_1-\varepsilon_2$. The Cooperon type diagrams $\mathcal{S}_n^{(C)}$ are defined by

$$\begin{aligned}\mathcal{S}_n^{(C)}(\omega;H)&=\mathrm{Tr}[\,\zeta^{(C)}(\omega;H)]^n\\&=\left(\int\prod_{j=1}^{n}d^dr_j\right)\prod_{m=1}^{n}\zeta^{(C)}(\mathbf{r}_m,\mathbf{r}_{m+1};\omega;H),\end{aligned} \tag{9}$$

with $\mathbf{r}_{n+1}\equiv\mathbf{r}_1$ and

$$\begin{aligned}&\zeta^{(C)}(\mathbf{r}_1,\mathbf{r}_2;\omega;H)\\&\quad=\frac{\hbar}{2\pi\nu\tau}G^+(\mathbf{r}_1,\mathbf{r}_2;\varepsilon_1;H)G^-(\mathbf{r}_1,\mathbf{r}_2;\varepsilon_2;H).\end{aligned} \tag{10}$$

Here $G^{+(-)}=\langle\mathcal{G}^{+(-)}\rangle_d$ is the disorder-averaged single-particle Green function. An example, $\mathcal{S}_4^{(C)}$, is shown schematically in Fig. 1(a). Note that the sum of diagrams $\mathcal{S}_n^{(C)}$ is equivalent to a number of one-loop diagrams in the conventional notation: they include the dominant contribution to $\tilde{K}^d$ in the diffusive regime for $d>2$ (Ref. 21), but are actually smaller than some two-loop diagrams in a wide region of energies in the diffusive regime at $d=2$ (Ref. 22). However in the region of interest of this paper, the nondiffusive ''ballistic'' regime, the diagrams $\mathcal{S}_n^{(C)}$ dominate.

B. Semiclassical treatment

Due to the lack of translational invariance in confined systems, it is no longer convenient to evaluate diagrams such as that in Fig. 1 in momentum space. Instead we work in configuration space and compute integrals (9), invoking a semiclassical approximation.

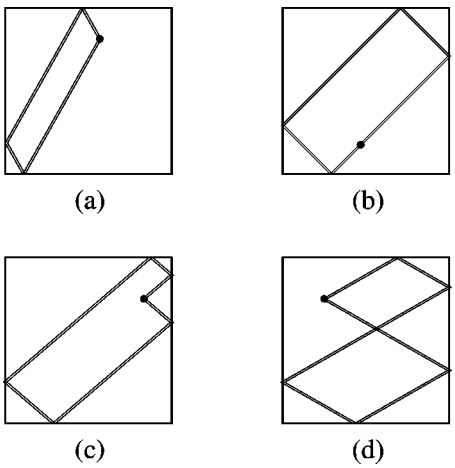

FIG. 2. Examples of diagonal pairs of real-space trajectories with one impurity scattering position in a square. (a), (c), and (d) show pairs of typical recurrent orbits with momentum exchange at the impurity which contribute to $\langle\chi^d(H)\rangle$, whereas (b) shows a pair of orbits following periodic orbits of the corresponding clean system which contribute to $\langle\chi^L(H)\rangle$.

Semiclassically, the single-particle Green function $\mathcal{G}^+(\mathbf{r}_1,\mathbf{r}_2)$ can be expressed as a sum over classical trajectories t between $\mathbf{r}_1$ and $\mathbf{r}_2$.[23] After disorder averaging, it reads[4]

$$G^+(\mathbf{r}_1,\mathbf{r}_2)\simeq\sum_{t:\mathbf{r}_1\to\mathbf{r}_2}D_t\exp\left(\frac{i}{\hbar}S_t(\mathbf{r}_1,\mathbf{r}_2)-\frac{L_t}{2l}\right). \tag{11}$$

The classical amplitude D_t includes the local density of trajectories near the path t, S_t stands for the classical action along the orbit including the Maslov index, and L_t is the orbit length. Equation (11) was derived in a semiclassical framework under the assumption that weak disorder modifies merely the phases S_t, which leads to damping on the scale of l, leaving the trajectories unaffected; i.e., the sum is taken over the paths of the corresponding clean system.

For the bulk case this treatment is equivalent to the usual diagrammatic treatment of disorder:[4] For white noise the self-consistent Born approximation leads to the following integral equation for the impurity-averaged single-particle Green function:[24]

$$\begin{aligned}G^+(\mathbf{r}_1,\mathbf{r}_2)&=\mathcal{G}^+(\mathbf{r}_1,\mathbf{r}_2)+\frac{\hbar}{2\pi\nu\tau}\\&\quad\times\int d\mathbf{r}_3\mathcal{G}^+(\mathbf{r}_1,\mathbf{r}_3)G^+(\mathbf{r}_3,\mathbf{r}_3)G^+(\mathbf{r}_3,\mathbf{r}_2).\end{aligned} \tag{12}$$

In the bulk case $G^+(\mathbf{r}_3,\mathbf{r}_3)$ in the above equation is given in terms of ''paths of zero length'' leading to the exponential damping of the (free) Green function without disorder. For confined systems further paths of finite length may semiclas-

sically contribute to $G^+(\mathbf{r}_3,\mathbf{r}_3)$. They can be viewed as paths scattered off the impurities which may lead to additional corrections to the impurity averaged single particle Green function. However, these contributions are of higher order in $\hbar$ and $1/\tau$.[25]

Upon using the semiclassical expression (11) in Eq. (10), the two-particle operator $\zeta^{(C)}(\mathbf{r}_1,\mathbf{r}_2;\omega;H)$ is then given in terms of a double sum over pairs of classical paths which explicitly include the effect of boundary scattering. However, most pairs (of different paths) produce oscillating contributions which we assume to vanish after energy or size averaging.[26] Therefore the main contribution to the field-sensitive part of $\langle K^d\rangle_L$ arises from diagonal terms (otherwise known as the Cooperon channel) obtained by pairing paths with their time reverse. Assuming that the magnetic field affects the phase of the particles but not their trajectories, for the actions we can write

$$\frac{1}{\hbar}S_t(\epsilon_i;H)\simeq\frac{1}{\hbar}S_t(E_F;H=0)+(\epsilon_i-E_F)T_t+\frac{2\pi}{\varphi_0}\int_{\mathbf{r}_1}^{\mathbf{r}_2}\mathbf{A}\cdot\mathbf{dr}, \tag{13}$$

where T_t is the period of the trajectory, $\mathbf{A}$ is the vector potential, and $\varphi_0=hc/e$. The diagonal approximation for $\zeta^{(C)}$ then gives

$$\zeta^{(C)}(\mathbf{r}_1,\mathbf{r}_2;\omega;H)=\sum_{t:\mathbf{r}_1\to\mathbf{r}_2}\tilde{\zeta}_t^{(C)}(\mathbf{r}_1,\mathbf{r}_2;\omega;H), \tag{14}$$

where

$$\tilde{\zeta}_t^{(C)}(\mathbf{r}_1,\mathbf{r}_2;\omega;H)\simeq\frac{v_F|D_t|^2}{2\pi\overline{\nu}\overline{l}}\exp\left[-\frac{L_t}{L_\phi}-\frac{L_t}{l}+i\omega T_t+i\frac{4\pi}{\varphi_0}\int_{\mathbf{r}_1}^{\mathbf{r}_2}\mathbf{A}\cdot\mathbf{dr}\right]. \tag{15}$$

The level broadening [implicit in L_ϕ, Eq. (5)] was introduced via $\omega\to\omega+i\gamma$. Equation (15) depends, besides l, only on the system without disorder, and holds for both integrable and chaotic geometries.

C. Disorder-induced magnetic response

Using Eqs. (3) and (8), the disorder-induced contribution to the average magnetic susceptibility is given by ($\varphi=HL^2/\varphi_0$)

$$\frac{\langle\chi^d(\varphi)\rangle}{|\chi_L|}\approx-\frac{6}{\pi^2}\frac{\partial^2}{\partial\varphi^2}\sum_{n=1}^{\infty}\frac{1}{n}\mathcal{S}_n^{(C)}(0;\varphi), \tag{16}$$

where the bulk Landau susceptibility is $\chi_L=-e^2/24\pi mc^2$ for spinless electrons.

Assuming that l remains fixed as k_FL changes, one sees from Eqs. (15) and (16) that $\langle\chi^d(\varphi)\rangle$ contains the dimensionless variables γ/Δ and k_FL only in the combination $(\gamma/\Delta)/k_FL$, since they are absorbed into the dimensionless variable L_ϕ/L [Eq. (5)]. It is now assumed that $\mathcal{S}_n^{(C)}$ in Eq. (16) contain diagonal terms only. Therefore, the propagator $\zeta^{(C)}$ [Eq. (14)] is made up of a summation over all diagonal pairs of paths including boundary scattering between any two given impurities situated at $\mathbf{r}_1$ and $\mathbf{r}_2$. On taking the trace over n propagators $\zeta^{(C)}$, one sees that the field sensitive part of S_n [Eq. (9)] consists of a summation over flux-enclosing pairs of closed paths (in position space) involving n impurities and an arbitrary number of boundary scattering events. An example of a pair of paths contributing to $\mathcal{S}_4^{(C)}$ is shown in Fig. 1(b).

III. INTEGRABLE GEOMETRIES: SQUARE BILLIARDS

In the following we apply the above formalism to compute the magnetic response of an ensemble of disordered billiards with regular geometry. We illustrate the method and present numerical results for the case of square billiards.

A. Numerical technique

We consider specular reflection at the boundaries and employ the extended zone scheme[20,27] to write $\zeta^{(C)}(\mathbf{r}_1,\mathbf{r}_2;\omega;H)$ [Eq. (14)] as a sum of propagators along *straight-line paths* $\tilde{\zeta}_t^{(C)}(\mathbf{r}_1,\mathbf{r}_2^t;\omega;H)$, of the form Eq. (15), where $\mathbf{r}_2^t$ are images of the position $\mathbf{r}_2$. The diagrams $\mathcal{S}_n^{(C)}$ [Eq. (9)] are then calculated by diagonalizing $\zeta^{(C)}$. At zero magnetic field this approach enables one to recover the result of Ref. 3 for the approximate diagonalization of the spectral correlation function $K^d(\varepsilon_1,\varepsilon_2;H=0)$, as outlined in the Appendix.

For a finite magnetic field the integrals over the magnetic vector potential along the paths do not allow for an analytical diagonalization of $\zeta^{(C)}$. However, we are able to use the fact that all variations of $\zeta^{(C)}$ occur on classical length scales; rapid oscillations on the scale of λ_F cancel out. This enables an efficient numerical computation. To this end we discretize the configuration space of the square billiard using a lattice with grid size greater than λ_F. By summing over all trajectories (up to a length $\gg L_\phi$) which connect two lattice cells, we compute the corresponding matrix elements of $\zeta^{(C)}$ in this representation. After diagonalization we obtain $\langle\chi^d(H)\rangle$ from Eq. (16).[28] This method is not restricted to the square geometry, but can be in principle applied to any geometry.

Note that the diagrams $\mathcal{S}_n^{(C)}$ do not include closed pairs of paths which follow periodic orbits of the corresponding clean system. Such paths involve zero momentum transfer between the Green functions at the impurity positions. They actually represent disconnected diagrams and are included in $\langle\chi^L(H)\rangle$, which was computed in Ref. 4. It is the presence of these periodic orbits in the determination of $\langle\chi^L(H)\rangle$ that leads to strong sensitivity of the orbital magnetism with respect to the system geometry.[29,27,30] The above numerical procedure does not distinguish between connected contributions to $\mathcal{S}_1$, with momentum exchange at the impurity as in Figs. 2(a), 2(c), 2(d), and disconnected diagrams involving one common impurity position. The dominant disconnected diagrams arise from the shortest flux enclosing periodic orbits of length $L_t=2\sqrt{2}L$ [Fig. 2(b)], and their repetitions. An estimate of their magnitude is obtained following the approach of RUJ.[4,27] On summation over all repetitions of the fundamental orbit, we find

$$\frac{\langle\chi(0)\rangle_{\rm dis}}{|\chi_L|}\simeq\frac{8\sqrt{2}}{5\pi}\frac{L}{l}\frac{1}{\sinh^2[\sqrt{2}(L/l+L/L_\phi)]}. \tag{17}$$

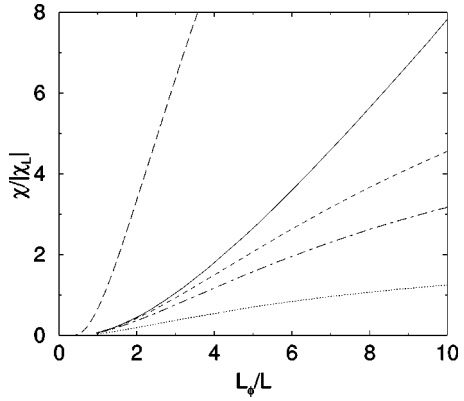

FIG. 3. Comparison of the relative contributions of diagrams $\mathcal{S}_n^{(C)}$ to $\langle\chi^d(0)\rangle$ for $l/L=4$ as a function of L_ϕ/L. The solid line corresponds to the inclusion of all diagrams while, from the bottom, the dotted line corresponds to $\mathcal{S}_1^{(C)}$ only, the dash-dotted line to $\mathcal{S}_1^{(C)}$ and $\mathcal{S}_2^{(C)}$, and the short dashed line to $\mathcal{S}_1^{(C)}$, $\mathcal{S}_2^{(C)}$, and $\mathcal{S}_3^{(C)}$. The long dashed line is the contribution of $\langle\chi^L(0)\rangle$.

To avoid double counting we explicitly subtract this estimation from the numerical determination of $\langle\chi^d(H)\rangle$.

B. Zero-field susceptibility

We briefly summarize our results for the magnetic susceptibility at zero field, and refer the reader to Ref. 5 for further details. The technique covers the whole range from the diffusive regime to the clean limit, and yields an averaged susceptibility which is always paramagnetic. In the diffusive limit, $l<L$, the disorder-induced susceptibility increases linearly with l in agreement with Ref. 31. In the ballistic regime, $\langle\chi^d(0)\rangle$ exhibits a maximum as a function of l/L. The occurrence of the maximum may be related to the competition between different effects of the impurity scattering on $\zeta^{(C)}$ [Eq. (15)]; while the single-particle Green functions are exponentially damped with l, l^{-1} enters into the prefactor.

In the elastic regime, $L<l<L_\phi$, $\langle\chi^d(0)\rangle$ exhibits a weak dependence on l, but is on the whole close to the prediction by GBM,[20] which is a paramagnetic l-independent contribution $\langle\chi^d(0)\rangle/|\chi_L|\approx 0.23\ k_F L(\Delta/\gamma)$. For larger l, in the inelastic regime, $L,L_\phi<l$, the susceptibility decays exponentially with both L/l and L/L_ϕ. The disorder-induced susceptibility $\langle\chi^d(0)\rangle$ for $l/L=4$ and a range of L_ϕ/L including both the elastic and inelastic regimes is shown as the solid line in Fig. 3. We also include the contributions of diagrams $\mathcal{S}_n^{(C)}$ [Eq. (9)] with a different number n of impurity scattering events in order to analyze their relative weights. From the bottom, the dotted line corresponds to $\mathcal{S}_1^{(C)}$ only, the dash-dotted line to $\mathcal{S}_1^{(C)}$ and $\mathcal{S}_2^{(C)}$, and the short dashed line to $\mathcal{S}_1^{(C)}$, $\mathcal{S}_2^{(C)}$, and $\mathcal{S}_3^{(C)}$. For completeness, the long dashed line is the contribution of $\langle\chi^L(0)\rangle$ (see below). The solid line curve shows linear behavior in the elastic regime, as predicted by GBM, and exponential behavior in the inelastic regime. In the limit $L_\phi\ll l$, where $\langle\chi^d(0)\rangle$ is very small, the lowest n diagrams dominate, but for $L_\phi>l$ a number of diagrams contribute significantly. We note that, contrary to what was stated in Ref. 3, the contribution from $\mathcal{S}_1^{(C)}$ is not particularly small through the whole range of L/L_ϕ.

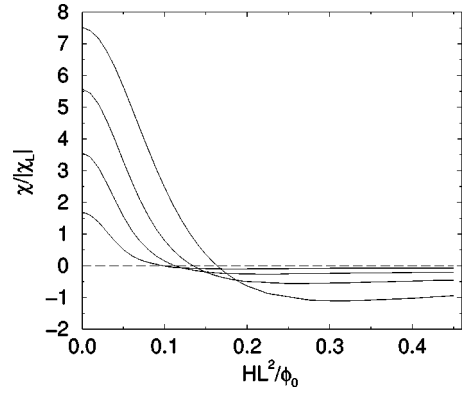

FIG. 4. Field-dependent susceptibility $\langle\chi^d(H)\rangle$ for a square for $k_F L=60$ and $\gamma/\Delta=1$ ($L_\phi/L=9.55$). From the top (at $H=0$), the mean free path is $l/L=5$, 10, 20, and 50.

C. Finite-field susceptibility

We compute the finite-field susceptibility $\langle\chi^d(H)\rangle$ for weak fields, assuming that the field does not perturb trajectories away from their zero-field straight line paths; i.e., we assume $r_c>l$, where $r_c=\hbar k_F c/eH$ is the cyclotron radius. Figure 4 shows $\langle\chi^d(H)\rangle$ for $k_F L=60$ and $\gamma/\Delta=1$ ($L_\phi/L=9.55$). From the top (at $H=0$), the mean free path is $l/L=5$, 10, 20, and 50. As the field increases from $H=0$ the susceptibility falls in magnitude and eventually becomes diamagnetic. The field value at which the susceptibility crosses over to diamagnetic behavior decreases as l/L increases. This implies that the typical area enclosed by a pair of recurrent orbits increases with l. In the range of validity of the above approach, $l<r_c, k_F L^2$ and $\gamma\gtrsim\Delta$, we do not observe oscillations of $\langle\chi^d(H)\rangle$ as a function of field as seen by GBM (Ref. 20) (albeit for a smaller value of γ/Δ).

D. Comparison of the combined semiclassical contributions with quantum-mechanical results

In this section we compare semiclassical results for $\langle\chi^d(H)\rangle$ and $\langle\chi^L(H)\rangle$ with numerical quantum calculations taken from Ref. 4. In order to obtain an analytic expression for the contribution of size-induced correlations $\langle\chi^L(H)\rangle$,[5] we employ the results of RUJ (Refs. 4 and 27) at zero temperature, and introduce the level broadening γ in the same way as for the disorder correlations. It has been shown[29,27] that the low-field susceptibility of an ensemble of *clean* squares is dominated by the shortest flux enclosing periodic orbits of length $L_t=2\sqrt{2}L$ and their repetitions over a broad range of temperature (or correspondingly inelastic scattering strengths). For the ballistic white noise case considered here, the effect of disorder averaging on the susceptibility was described by an additional damping $\exp(-L_t/l)$ of the response of the clean system.[4] This result corresponds to $\langle\chi^L(H)\rangle$ including the disorder damping $\exp(-L_t/2l)$ of the two single-particle Green functions.

The numerical quantum calculations[4] were obtained by diagonalization of the Hamiltonian for noninteracting spinless particles in a square billiard with perpendicular magnetic field and white noise random potential. In this calculation temperature smearing, rather than level broadening due to inelastic effects, was introduced.

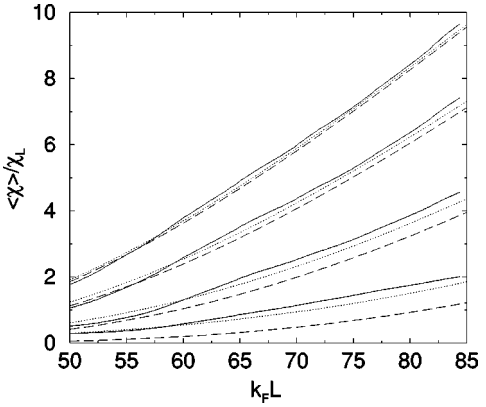

FIG. 5. Disorder- and size-induced contributions to the susceptibility. The mean susceptibility for small field, $\varphi=0.15$, and high temperature $k_BT/\Delta=2$ ($L_T/L\approx1.8$ at $k_FL=70$), for various disorder strengths, taking into account the variation of the mean free path with k_F; $l\propto k_F$. From the top, the elastic mean free path is $l/L=8,4,2$, and 1 (at $k_FL\approx70$). The full and dashed curves are data from a quantum-mechanical calculation and from a semiclassical evaluation of the contribution of size-induced correlations, respectively, taken from Ref. 4. The dotted curve represents the sum of our semiclassical evaluation of the disorder-induced correlations, using $\gamma/\Delta\approx\pi k_BT/\Delta$, and the semiclassical data for size-induced correlations from Ref. 4.

The full lines in Fig. 5 show the numerical results for various disorder strengths as a function of k_FL. From the top, the elastic mean free path is $l/L=8,4,2$, and 1 (at $k_FL\approx70$). As k_FL changes, the mean free path is assumed to change also, according to $l\propto k_F$.

The dashed curves in Fig. 5 are data taken from Ref. 4 for the semiclassical evaluation of the contribution of size-induced correlations to the susceptibility, $\langle\chi^L(H)\rangle$. We calculated the contribution of the disorder-induced correlations, $\langle\chi^d(H)\rangle$, using the approximation[32] $\gamma/\Delta\approx\pi k_BT/\Delta$, and taking into account the variation of mean free path with k_FL. The resulting semiclassical evaluation of the total susceptibility, $\langle\chi^L(H)\rangle+\langle\chi^d(H)\rangle$, is obtained by adding our results to those given by the dashed curves; the results are shown as dotted curves in Fig. 5.

For $k_FL\gtrsim60$ the agreement of the semiclassical (dotted) curves with the quantum results is considerable; it is clear that the difference between the semiclassical results for $\langle\chi^L(H)\rangle$ and the quantum results is accounted for by the addition of $\langle\chi^d(H)\rangle$. However, even for $k_FL\gtrsim60$ the agreement is not exact; we believe that this minor discrepancy is due to the different mechanisms of damping that were used.

For $k_FL\lesssim60$ there is worse agreement between the semiclassical (dotted) curves and the quantum results. This may be related to the fact that the semiclassical results show no sign of the oscillatory structure present in the quantum curves. This structure may be caused by off-diagonal pairs of different families of short periodic orbits contributing to $\langle\chi^L(H)\rangle$, which are not completely suppressed through energy average and are not included in the present semiclassical approach.

E. Relation to experiment

Measurements of the orbital magnetism of ballistic systems, which are experimentally realized as semiconductor microstructures, are still rare.[8,9] In the experiment of Ref. 9 the susceptibility of ensembles of squares was studied. The samples used had estimated values for the elastic mean free path of $l/L\sim1-2$, for the phase-coherence length of $\sim(3-10)L$ and for a thermal cutoff length of $L_T/L\sim2$. Therefore, the length scale L_ϕ [Eq. (5)] is determined by the shorter length L_T. Figure 5 shows that for these experimental parameters both the disorder and size-induced correlations are relevant; however, the latter contribution is dominant.

The above remarks hold for white noise disorder. However, experimental ballistic structures such as those of Ref. 9 are usually characterized by smooth disorder potentials. Smooth disorder effects can be in principle incorporated into the present calculation by introducing an angle-dependent cross section for the impurity scattering between two successive trajectory segments. The effect of smooth disorder on $\langle\chi^L\rangle$ was analyzed in Ref. 4, which showed that the reduction of the clean contribution is not as strong as that for white noise disorder, and no longer exponential. We therefore expect that in the parameter regime of the experiment the domination of the susceptibility by size-induced correlations is further enhanced when considering smoothed disorder.

The measured value of the susceptibility at *low* temperature was $\chi(0)\sim100|\chi_L|$, with an uncertainty of about a factor of 4. The combined contributions $\langle\chi^d\rangle$ and $\langle\chi^L\rangle$, together with an interaction contribution of the same order,[33] are in broad agreement with the experimental result. We note, however, that a theoretical explanation of the temperature dependence of the measured susceptibility is still lacking.

IV. CHAOTIC GEOMETRIES

For systems with a generic chaotic, clean counterpart we obtain an analytical estimate for $\langle\chi^d(0)\rangle$ under certain statistical assumptions with respect to the classical trajectories involved. To this end we make use of the relation[17] (L^2 denotes the system area)

$$\frac{\hbar}{\pi\nu}\sum_{j:\mathbf{r}_1\to\mathbf{r}_2}|D_j|^2\delta(t-t_j)=P(\mathbf{r}_1,\mathbf{r}_2;t) \tag{18}$$

in order to transform the sums over classical densities $|D_t|^2$ in Eq. (15) into classical probabilities $P(\mathbf{r}_1,\mathbf{r}_2;t)$ to propagate classically between impurities at $\mathbf{r}_1$ and $\mathbf{r}_2$ in time t.

In the following we assume that in the ''ballistic'' regime $l,L_\phi\gg L$ the conditional probability $P(\mathbf{r}_1,\mathbf{r}_2;t|\mathcal{A})$ to accumulate an ''area'' $\mathcal{A}$ during the propagation from $\mathbf{r}_1$ and $\mathbf{r}_2$ is independent of $\mathbf{r}_1$ and $\mathbf{r}_2$. Following Ref. 29, which considered clean billiards, we find, from Eqs. (15) and (18),

$$\zeta^{(C)}(\mathbf{r}_1,\mathbf{r}_2;\omega;H)\simeq\frac{1}{\tau}\int_0^\infty dt\int_{-\infty}^{\infty}d\mathcal{A}\,P(\mathbf{r}_1,\mathbf{r}_2;t|\mathcal{A})\cos\left(\frac{4\pi\mathcal{A}H}{\varphi_0}\right)\exp\left[-\gamma t-\frac{t}{\tau}+i\omega t\right]. \tag{19}$$

We assume that after several bounces off the boundary the area distribution $P(\mathbf{r}_1,\mathbf{r}_2;t|\mathcal{A})$ becomes Gaussian with a variance σ independent of $\mathbf{r}_1$ and $\mathbf{r}_2$ and independent of l. Substituting the above expression for $\zeta^{(C)}$ into Eq. (9), and performing the r, t, and $\mathcal{A}$ integrals, we obtain the following closed approximate form for $\mathcal{S}_n^{(C)}$:

$$\mathcal{S}_n^{(C)}(\omega;H)\approx\left\{\frac{8\pi^2H^2l\sigma}{\varphi_0^2}+1+\gamma\tau-i\omega\tau\right\}^{-n}. \tag{20}$$

Summation of the $\mathcal{S}_n^{(C)}$ [Eq. (16)] leads to the disorder-induced contribution to the average susceptibility,

$$\frac{\langle\chi^d(\varphi)\rangle}{|\chi_L|}\approx-\frac{24}{\varphi_0^2}\frac{\partial^2}{\partial\varphi^2}\ln\left\{\frac{\frac{8\pi^2\varphi^2l\sigma}{L^4}+\frac{l}{L_\phi}}{1+\frac{8\pi^2\varphi^2l\sigma}{L^4}+\frac{l}{L_\phi}}\right\}, \tag{21}$$

where $\varphi=HL^2/\varphi_0$. It is possible to obtain an explicit expression for $\langle\chi^d(\varphi)\rangle$ analytically. For brevity we give only the limits.

The susceptibility has a paramagnetic maximum for zero field,

$$\frac{\langle\chi^d(0)\rangle}{|\chi_L|}\simeq\frac{96\sigma L_\phi^2}{L^4(L_\phi+l)}, \tag{22}$$

and it changes sign only once, for example in the elastic regime at the critical flux:

$$\varphi_c^2\approx\frac{L^3}{8\pi^2\sigma(L_\phi/L)},\quad L_\phi>l. \tag{23}$$

For a large field, $\varphi\gg\varphi_c$, the susceptibility remains diamagnetic and decays rapidly:

$$\frac{\langle\chi^d(\varphi)\rangle}{|\chi_L|}\sim-\frac{6L^3}{\pi^4\sigma(l/L)\,\varphi^4}. \tag{24}$$

The susceptibility as a function of field is plotted in Fig. 6 for $k_FL=60$ and $\gamma/\Delta=1$ ($L_\phi/L=9.55$). Various disorder strengths are shown, from the top (at $H=0$), $l/L=5$,10,20, and 50. These curves are qualitatively similar to those for the square geometry shown in Fig. 4. This may be related to the fact that for trajectories being (multiply) scattered at impurities the character of the clean geometry, namely, regular or chaotic, is of minor importance. Note, however, that the classical variance σ determines the height and the correlation field φ_c.

The susceptibility $\langle\chi^d(0)\rangle$ as a function of L_ϕ for $l/L=2$ is shown as the dash-dotted line in Fig. 7 and a corresponding approximation for $\langle\chi^L(0)\rangle$ (Ref. 27) for finite L_ϕ,

$$\frac{\langle\chi^L(0)\rangle}{|\chi_L|}\simeq\frac{96\sigma L_\phi l}{L^4(L_\phi+l)}, \tag{25}$$

is shown as the short dashed line in Fig. 7. The two contributions [Eqs. (22) and (25)] add up to an *l-independent* magnetic response

$$\frac{\langle\chi(0)\rangle}{|\chi_L|}\simeq\frac{96\sigma L_\phi}{L^4}, \tag{26}$$

which is the same as that for clean chaotic systems, given the assumption of an l-independent variance.

For comparison, results for the square geometry as a function of L_ϕ for $l/L=2$ are also presented in Fig. 7. The solid line shows our numerical results for $\langle\chi^d(0)\rangle$, and the long dashed line shows $\langle\chi^L(0)\rangle$ (see Ref. 5 for more details). The L_ϕ dependence also shows a qualitative similarity between the disorder-induced susceptibility in the square geometry

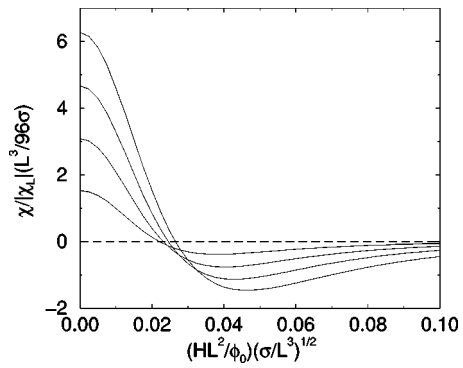

FIG. 6. Field-dependent susceptibility $\langle\chi^d(H)\rangle$ (normalized) for a generic chaotic geometry for $k_FL=60$ and $\gamma/\Delta=1$ ($L_\phi/L=9.55$). From the top (at $H=0$), the mean free path is $l/L=5$, 10, 20, and 50.

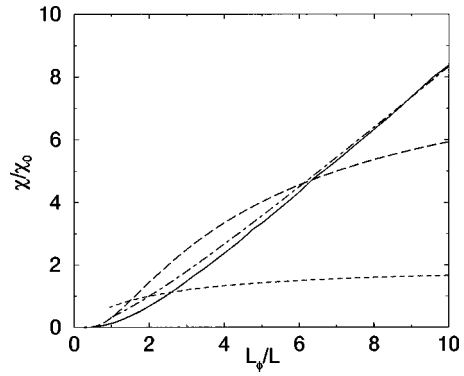

FIG. 7. Contributions to the susceptibility for $k_FL=60$ and $l/L=2$, with (normalized) semiclassical estimates for $\langle\chi^d(0)\rangle$ (dash-dotted line) and $\langle\chi^L(0)\rangle$ (short dashed line) for a generic chaotic geometry and for $\langle\chi^d(0)\rangle$ (solid line) and $\langle\chi^L(0)\rangle$ (long dashed line) for a square geometry. $\chi_0=|\chi_L|$ for the square geometry and $|\chi_L|L^3/96\sigma$ for the chaotic geometry.

and the chaotic geometry. Naturally, the square and the chaotic billiard show quite different behaviors for the size-induced susceptibility. For the square a crossover from domination by disorder-induced correlations to domination by size-induced correlations occurs for $L_\phi \sim l^2$, which contrasts with chaotic geometries where the crossover occurs for $L_\phi = l$.

V. CONCLUDING REMARKS

We considered disorder-induced spectral correlations of mesoscopic quantum systems in the nondiffusive regime. We combined a diagrammatic treatment of the disorder with a semiclassical approach for the Green functions involved. This leads to a representation of the diagrams involved in terms of (pairs of) classical paths in real space which undergo both (multiple) scattering at the impurities and reflections at the system boundaries. This hybrid-type approach enables us to perform disorder and energy averages, and to study the complete crossover from the diffusive to the clean limit for arbitrary values of the elastic mean free path l and L_ϕ (smaller than $v_F t_H$). In particular, it is applicable to ballistic microstructures of, in principle, arbitrary geometry. The approach, presented here for billiard systems, also applies to systems with potentials whose effect is then incorporated into the semiclassical Green functions.

We focused on the effect of disorder-induced correlations on the averaged magnetic susceptibility which is closely related to the spectral number variance, and which amounts to evaluating Cooper-type contributions to the correlator. Corresponding diffuson-type diagrams can be computed equivalently. As an example of a system with an integrable clean counterpart, we treated in detail the (experimentally relevant) square billiard. We showed that there are two distinct regimes of behavior depending on the relative magnitudes of l and L_ϕ. Certain statistical assumptions on the trajectories in ballistic systems with a generic chaotic geometry enabled us to derive approximate analytical expressions for the disorder-induced magnetic response. It turns out that the magnetic-field dependence and L_ϕ dependence of the susceptibility, at least qualitatively, resemble that of the integrable case. This implies that the actual geometry of the clean system is of minor importance for the disorder-induced orbital magnetism even in the ballistic regime.

ACKNOWLEDGMENTS

We are grateful to Y. Gefen, S. Kettemann, D. E. Khmelnitskii, M. Leadbeater, I. V. Lerner, and P. Walker for useful discussions. We thank the Isaac Newton Institute for Mathematical Sciences, Cambridge, where part of this research was performed.

APPENDIX: DIAGONALIZATION OF ζ OPERATORS FOR ZERO FIELD

In this appendix we show that within the semiclassical approach the analytical diagonalization of the ζ operators [Eq. (10)] for a square geometry at zero field is possible and straightforward. We employ the extended zone scheme which is constructed by reflecting the original billiard with respect to its boundaries. Any given trajectory connecting $\mathbf{r}_1 \equiv (x_1, y_1)$ and $\mathbf{r}_2 \equiv (x_2, y_2)$ involving an arbitrary number of specular reflections at the boundaries is transformed into a straight-line path connecting $\mathbf{r}_1$ and $\mathbf{r}_2^t$, where $\mathbf{r}_2^t \equiv (\pm x_2 + 2n_x L, \pm y_2 + 2n_y L)$ is an image of the position $\mathbf{r}_2 \equiv (x_2, y_2)$, and n_x and n_y are integers. As a result a semiclassical propagator $\zeta^{(C)}(x_1, y_1; x_2, y_2)$ may be written as a sum of propagators, $\tilde{\zeta}^{(C)}(x_1, y_1; x_2^t, y_2^t)$, along straight-line trajectories,

$$\zeta^{(C)}(x_1,y_1;x_2,y_2) = \sum_{n_x=-\infty}^{\infty} \sum_{n_y=-\infty}^{\infty} \tilde{\zeta}^{(C)}(x_1,y_1;\pm x_2 + 2n_x L, \pm y_2 + 2n_y L). \tag{A1}$$

Since $\tilde{\zeta}^{(C)}$ is dependent only on the distances $X \equiv (x_2^t - x_1)$ and $Y \equiv (y_2^t - y_1)$ along a straight line it is possible to introduce a Fourier transform $\lambda(q_x, q_y)$ and, using the Poisson summation rule, we may write

$$\zeta^{(C)}(x_1,y_1;x_2,y_2) = \sum_{m_x, m_y=-\infty}^{\infty} \int_{-\infty}^{+\infty} \frac{dq_x dq_y}{(2\pi)^2} 4\,\lambda(q_x,q_y)\cos(q_x x_1)\cos(q_y y_1)\,\delta\left(\frac{q_x L}{\pi} - m_x\right)\delta\left(\frac{q_y L}{\pi} - m_y\right) e^{\{iq_x x_2 + iq_y y_2\}}. \tag{A2}$$

Performing the integrals gives quantized momentum values $q_x = m_x \pi / L$, $q_y = m_y \pi / L$ and

$$\zeta^{(C)}(x_1,y_1;x_2,y_2) = \frac{1}{L^2}\Bigg[\lambda(0,0) + 4\sum_{m_x=1}^{\infty}\sum_{m_y=1}^{\infty} \lambda\left(\frac{m_x\pi}{L}, \frac{m_y\pi}{L}\right)\cos\left(\frac{m_x\pi x_1}{L}\right)\cos\left(\frac{m_y\pi y_1}{L}\right)\cos\left(\frac{m_x\pi x_2}{L}\right)\cos\left(\frac{m_y\pi y_2}{L}\right)$$
$$+ 2\sum_{m_x=1}^{\infty} \lambda\left(\frac{m_x\pi}{L}, 0\right)\cos\left(\frac{m_x\pi x_1}{L}\right)\cos\left(\frac{m_x\pi x_2}{L}\right) + 2\sum_{m_y=1}^{\infty} \lambda\left(0, \frac{m_y\pi}{L}\right)\cos\left(\frac{m_y\pi y_1}{L}\right)\cos\left(\frac{m_y\pi y_2}{L}\right)\Bigg]. \tag{A3}$$

Although $\zeta^{(C)}(x_1, y_1; x_2, y_2)$ is not translationally invariant, it does have a periodicity of $2L$. The diagrams $\mathcal{S}_n$ may be written in terms of the Fourier transform $\lambda(q_x, q_y)$ by inserting the above expression into Eq. (9). Spatial integrals are performed using the following relation:

$$\int_0^L \frac{dx}{L}\cos\left(\frac{m_x \pi x}{L}\right)\cos\left(\frac{m_{x'}\pi x}{L}\right) = \frac{1}{2}(\delta_{m_x,m_{x'}} + \delta_{m_x,-m_{x'}}), \tag{A4}$$

and the result is

$$\mathcal{S}_n^{(C,D)} = \sum_{m_x=0}^{\infty}\sum_{m_y=0}^{\infty}\left[\lambda\left(\frac{m_x\pi}{L},\frac{m_y\pi}{L}\right)\right]^n. \tag{A5}$$

In order to evaluate $\lambda(q_x,q_y)$, we Fourier transform the expression for the semiclassical operator $\tilde{\zeta}_t^{(C)}$ [Eq. (15)] performing integrals over X and Y. By changing from Cartesian coordinates (X,Y) to polar coordinates (r,θ), the radial integration is done, giving

$$\lambda(q_x,q_y) = \frac{1}{2\pi}\int_0^{2\pi}\frac{d\theta}{(1+\gamma\tau - i\omega\tau) + il(q_x\cos\theta + q_y\sin\theta)}, \tag{A6}$$

and we find

$$\lambda(q_x,q_y) = \frac{1}{\sqrt{(1+\gamma\tau - i\omega\tau)^2 + (lq)^2}}, \tag{A7}$$

where $q^2 = q_x^2 + q_y^2$. This result is in agreement with the approximate diagonalization of Ref. 3. Together with Eq. (8), it gives the spectral correlation function in the ''ballistic'' regime.

*Present address: School of Physics and Chemistry, Lancaster University, Lancaster, LA1 FYB, UK.

[1] B. L. Altshuler, P. A. Lee, and R. A. Webb, *Mesoscopic Phenomena in Solids* (North-Holland, Amsterdam, 1991).

[2] U. Sivan and Y. Imry, Phys. Rev. B **35**, 6074 (1987).

[3] A. Altland and Y. Gefen, Phys. Rev. Lett. **71**, 3339 (1993); Phys. Rev. B **51**, 10 671 (1995).

[4] K. Richter, D. Ullmo, and R. A. Jalabert, J. Math. Phys. **37**, 5087 (1996); Phys. Rev. B **54**, R5219 (1996).

[5] E. McCann and K. Richter, Europhys. Lett. **43**, 241 (1998).

[6] For recent reviews on persistent currents in disordered rings see, e.g., K. Efetov, *Supersymmetry in Disorder and Chaos* (Cambridge University Press, Cambridge, 1996); U. Eckern and P. Schwab, Adv. Phys. **44**, 387 (1995). For reviews on orbital magnetism of ballistic structures see, e.g., Ref. 29 and K. Richter, *Springer Tracts in Modem Physics* (Springer, Berlin, in press).

[7] For the diffusive case, see L. P. Lévy, G. Dolan, J. Dunsmuir, and H. Bouchiat, Phys. Rev. Lett. **64**, 2074 (1990); V. Chandrasekhar, R. A. Webb, M. J. Brady, M. B. Ketchen, W. J. Gallagher, and A. Kleinsasser, *ibid.* **67**, 3578 (1991); P. Mohanty, E. M. Q. Jariwala, M. B. Ketchen, and R. A. Webb, in *Quantum Coherence and Decoherence*, edited by K. Fujikawa and Y. A. Ono (Elsevier, Amsterdam, 1996).

[8] D. Mailly, C. Chapelier, and A. Benoit, Phys. Rev. Lett. **70**, 2020 (1993).

[9] L. P. Levy, D. H. Reich, L. Pfeiffer, and K. West, Physica B **189**, 204 (1993).

[10] H. F. Cheung, Y. Gefen, E. K. Riedel, and W. H. Shih, Phys. Rev. B **37**, 6050 (1988).

[11] H. Bouchiat and G. Montambaux, J. Phys. (Paris) **50**, 2695 (1989).

[12] B. L. Altshuler, Y. Gefen, and Y. Imry, Phys. Rev. Lett. **66**, 88 (1991); A. Schmid, *ibid.* **66**, 80 (1991); F. von Oppen and E. K. Riedel, *ibid.* **66**, 84 (1991); E. Akkermans and B. Shapiro, Europhys. Lett. **11**, 467 (1990); E. Akkermans, *ibid.* **15**, 709 (1991). For the treatment of ballistic systems, see Ref. 29.

[13] P. G. de Gennes and M. Tinkham, Physics (Long Island City, NY) **1**, 107 (1964).

[14] C. W. J. Beenakker and H. van Houten, Phys. Rev. B **38**, 3232 (1998).

[15] V. K. Dugaev and D. E. Khmel'nitskii, Zh. Éksp. Teor. Fiz. **86**, 1784 (1984) [Sov. Phys. JETP **59**, 1038 (1984)].

[16] S. Chakravarty and A. Schmid, Phys. Rep. **140**, 193 (1986).

[17] N. Argaman, Y. Imry, and U. Smilansky Phys. Rev. B **47**, 4440 (1993).

[18] O. Agam and S. Fishman, Phys. Rev. Lett. **76**, 726 (1996).

[19] B. A. Muzykantskii and D. E. Khmelnitskii, Pis'ma Zh. Éksp. Teor. Fiz. **62**, 68 (1995) [JETP Lett. **62**, 76 (1995)].

[20] Y. Gefen, D. Braun, and G. Montambaux, Phys. Rev. Lett. **73**, 154 (1994); D. Braun, Y. Gefen, and G. Montambaux, Ann. Phys. (Leipzig) **3**, 467 (1994).

[21] B. L. Altshuler and B. I. Shklovskii, Zh. Éksp. Teor. Fiz. **91**, 220 (1986) [Sov. Phys. JETP **64**, 127 (1986)].

[22] V. E. Kravtsov and I. V. Lerner, Phys. Rev. Lett. **74**, 2563 (1995).

[23] M. C. Gutzwiller, *Chaos in Classical and Quantum Mechanics* (Springer, Berlin, 1990).

[24] A. D. Stone, in *Physics of Nanostructures*, edited by J. H. Davies and A. R. Long (Cromwell Press Ltd, Wiltshire, 1992).

[25] E. McCann and K. Richter (unpublished).

[26] In a ballistic system such additional oscillatory terms will however remain upon pure disorder average for fixed size (Refs. 3 and 4).

[27] D. Ullmo, K. Richter, and R. A. Jalabert, Phys. Rev. Lett. **74**, 383 (1995).

[28] A similar calculation has been applied to a different ''classical'' operator, describing interaction effects in ballistic quantum dots, in Ref. 33.

[29] K. Richter, D. Ullmo, and R. A. Jalabert, Phys. Rep. **276**, 1 (1996).

[30] A similar strong sensitivity with respect to the system geometry occurs in interacting ballistic quantum dots due to the presence of off-diagonal periodic orbit terms (Ref. 33).

[31] S. Oh, A. Y. Zyuzin, and R. A. Serota, Phys. Rev. B **44**, 8858 (1991).

[32] We note that a proper consideration (Ref. 25) of temperature smoothing by convoluting the spectral correlation functions with the Fermi function amounts to replacing the exponential damping with L_ϕ in Eq. (13) by the damping $x/\sinh x$ with $x = \pi T_t k_B T/\hbar$, where T_t is the period of the classical path involved, and T the temperature.

[33] D. Ullmo, H. U. Baranger, K. Richter, F. von Oppen, and R. A. Jalabert, Phys. Rev. Lett. **80**, 895 (1998).